Nuclear Engineering and Technology 55 (2023) 3983–3995

Contents lists available at ScienceDirect

Nuclear Engineering and Technology

journal homepage: www.elsevier.com/locate/net

Original Article

A reduced order model for fission gas diffusion in columnar grains

D. Pizzocri [a,*], M. Di Gennaro [a], T. Barani [a], F.A.B. Silva [b], G. Zullo [a], S. Lorenzi [a], A. Cammi [a]

[a] Politecnico di Milano, Department of Energy, Nuclear Engineering Division, Via La Masa 34, I-20156, Milano, Italy
[b] Eindhoven University of Technology, Department of Mathematics and Computer Science, Centre for Analysis, Scientific Computing and Applications, Netherlands

ARTICLE INFO

Keywords:
Fuel performance codes
Fission gas
Fast reactors
Reduced order model
SCIANTIX

ABSTRACT

In fast reactors, restructuring of the fuel micro-structure driven by high temperature and high temperature gradient can cause the formation of columnar grains. The non-spheroidal shape and the non-uniform temperature field in such columnar grains implies that standard models for fission gas diffusion can not be applied. To tackle this issue, we present a reduced order model for the fission gas diffusion process which is applicable in different geometries and with non-uniform temperature fields, maintaining a computational requirement in line with its application in fuel performance codes. This innovative application of reduced order models as meso-scale tools within fuel performance codes represents a first-of-a-kind achievement that can be extended beyond fission gas behaviour.

1. Introduction

During the normal operation of a nuclear power plant, the irradiation of the fuel determines the creation of gaseous fission products, mainly Xenon and Krypton, within the fuel grains. These gases tend to diffuse through the fuel polycrystalline matrix and are progressively released into the free volume of the fuel rod. The release of fission gases affects the performance of the fuel rod since their presence in the gap causes an increase in pressure, thus subjecting the cladding to stress, and deteriorates the thermal conductance of the gap, increasing the fuel temperature as well. Consequently, modeling of fission gas behaviour is essential in the frame of the thermo-mechanical analysis of fuel rods [1–6]. described by dedicated fuel performance codes (FPCs) [7,8].

Fuel performance codes are at the top of the hierarchical multi-scale modeling approach that goes from the atomistic scale to the engineering scale [9–12]. Physics-based approaches adopted in FPCs are often represented by a set of partial differential equations (PDEs) with parametric dependencies. Numerical simulations at the engineering scale of the integral fuel rod require high computational efforts, considering the long calculation times and the high number of information processed due to the various conditions encountered throughout the life of the fuel rod. Accordingly, there is a need to find a compromise between computational complexity and the accuracy of the numerical solution.

Several fast-running algorithms have been developed for the physics-based simulation of fission gas diffusion, such as FORMAS [13–15], the quasi-exact ANS-5.4 [15–18], URGAS [15,19], PolyPole-1 [20] and PolyPole-2 [21]. The widely used FORMAS algorithm adopts a linearization of the source and the diffusion term to take into account an expansion on the diffusion kernel. The quasi-exact ANS-5.4 algorithm is derived directly from the analytic solution of the diffusion equation for constant conditions and is affected only by discretization errors of real history into piecewise-constant conditions, for this reason, it is labeled ”quasi-exact” algorithm, making it a reference solution in many numerical experiments (the simulation of many power histories whose parameters, for example, the duration, the temperature, and the fission rate, are chosen randomly), as in Refs. [15,21,22], based on piecewise-constant power histories.

The main limitation of these algorithms is that they adopt the radial part of the spherical Laplacian as the diffusion operator making them specific for the problem related to the isotropic diffusion in the spherical grains of the irradiated uranium dioxide matrix in a light water reactor. Therefore, it is not possible to apply them directly in other conditions. For instance, in fast reactors where the high fuel temperature values determine an intense restructuring phenomenon with consequent formation of cylindrical grains [1,23,24], or in the case of uranium silicide [25], where we have to deal with an anisotropic diffusion dictated by the fuel tetragonal crystalline structure [26]. In particular, regarding the cylindrical grains, the steep temperature gradient established along them makes it necessary to use a diffusion coefficient dependent on the temperature profile. Moreover, the diffusion dynamics of fission gases in cylindrical grains is not comparable to that of spherical grains, given the geometrical difference.

* Corresponding author.
E-mail address: davide.pizzocri@polimi.it (D. Pizzocri).

https://doi.org/10.1016/j.net.2023.07.013
Received 24 January 2023; Received in revised form 22 June 2023; Accepted 9 July 2023
Available online 17 July 2023

Reduce order modelling (ROM) techniques allow replacing a high-fidelity problem with one of much lower complexity preserving the accuracy of the solution as much as possible [27]. Thus they are suitable to ensure low computational cost and hence applicability in fuel performance codes, while allowing to model a wide range of conditions and geometries. ROMs represent a cutting-edge topic in applied mathematics but their potential is not yet exploited in the field of fuel performance. The goal of this work is thus to develop a reduced order model for the diffusion process of fission gases applicable to spherical and cylindrical grains.

The reduced order technique adopted in this work is based on the use of intrusive-projection methods. The main assumption is that the variables of interest can be expressed as a linear combination of spatial modes multiplied by the time coefficients [28]. To construct an efficient reduced order model it is essential to select the correct spatial modes, for this reason, the proper orthogonal decomposition (POD) technique is herein adopted due to its ability to select the most energetic modes regardless of the geometry [29–31]. This technique is used to define the subspace of smaller dimension on which to project, through the Galerkin projection, the partial differential equation that governs the phenomenon of intra-granular fission gas diffusion. The set of spatial modes that populate the subspace can be built starting from *snapshots*, i.e., solutions of the diffusion equation obtained through high-fidelity numerical simulations at different instants. Another essential element is the subdivision of the computational procedure into an Offline phase in which the expensive computation of snapshots and the modes calculation can be performed just once and totally decoupled from the Online phase characterized by the fast-running ROM simulation.

The structure of the paper is as follows: In Section 2, the mathematical formulation of the intra-granular fission gas diffusion in both spherical and cylindrical grains is discussed. In Section 3 and Section 4 the two main elements of the Offline procedure are outlined, in particular the Full Order Model (FOM) and the ROM. In Section 5, we describe the implementation of the Online phase in the physics-based grain-scale code SCIANTIX [32,33] and its numerical verification. In Section 6, the ROM for spherical grains is verified by comparing it to other state-of-the-art algorithms used in fuel performance codes in terms of accuracy and computational efficiency. Conclusions and further development are outlined in Section 7.

2. Mathematical problem

The oxide fuel in fast reactors undergoes a restructuring process due to the high temperature and the high temperature gradient [1,24]. This process involves changes of the local porosity distribution (and in turn, of the local fuel density) within the fuel pellet and of the morphology of the grains, leading to the formation of three micro-structures within the fuel pellet. Radially, from the rim of the pellet towards its centre, three zones can be identified: (1) an external (roughly corresponding to temperature below 1600°C) as-fabricated zone (unchanged density); (2) an intermediate (from 1600°C to 1800°C) zone with equiaxed grains (higher density, grain-size of around 20 μm), and (3) an internal (above 1800°C) zone with columnar grains (almost theoretical density, grain length of roughly 1 mm). The columnar grains are formed by the migration of the pores towards the centre by a mechanism of evaporation-condensation across the pore faces [1,34–36]. The pores gather in the centre of the pellet forming a central void.

For both as-fabricated and equiaxed grains, the description of inert gas behaviour is not substantially different from that of unrestructured oxide fuel, since the geometry of the grains is essentially unchanged [37,38]. The classical description adopted in fuel performance codes relies on the equivalent sphere model proposed by Booth [38]. Thus exploiting the spherical symmetry of the problem and assuming that the grain size is small enough to assume uniform temperature and fission rate (and hence, uniform diffusivity and gas production rate) the governing equation of the intra-granular diffusion in fuel spherical grains can be written in this way:

$$\frac{\partial c(r_s,t)}{\partial t} = D(T,\dot{F})\frac{1}{r_s^2}\frac{\partial}{\partial r_s}\left(r_s^2\frac{\partial}{\partial r_s}c(r_s,t)\right) + S \tag{1}$$

where t (s) is time, $c\left(\text{at m}^{-3}\right)$ is the intra-granular gas concentration, r_s (m) is the radial coordinate in the spherical grain, $D\left(\text{m}^2\ \text{s}^{-1}\right)$ is the isotropic gas atom diffusion coefficient[1], T (K) is the temperature, and $S\left(\text{at m}^{-3}\ \text{s}^{-1}\right)$ is the production rate of fission gas which is in turn given by the fission rate density $\dot{F}\left(\text{fiss m}^{-3}\ \text{s}^{-1}\right)$ multiplied by the total yield of fission gas atoms $y\left(\text{at fiss}^{-1}\right)$. The analytic solution of the average gas concentration is well known [15,20].

Treating columnar grains according to Eq. (1), even considering a made up size of the sphere representative of the cylinder, incurs in two main issues: (i) the dynamics of diffusion are different in a sphere and in a cylinder and cannot be set equal by the selection only of a representative spherical grain radius; and (ii) given the temperature dependence of the diffusion coefficient and the temperature profile in the columnar zone, the use of a single value for the diffusion coefficient is inaccurate. Therefore, the assumption of spherical grains in Eq. (1), hinders *a priori* the application of this diffusion description to columnar grains.

To properly account for the effects of steep temperature gradients along the columnar grain axis (i.e., the temperature gradient along the radius of the pellet, around 200°C mm^{-1}), the physical problem of gas diffusion must be coupled to a 1D heat-diffusion model for the temperature distribution over the z axis of the grain. This results in the system of coupled partial differential equations:

$$\begin{cases} \dfrac{\partial T(z,t)}{\partial t} = \alpha\dfrac{\partial}{\partial z}\left(\dfrac{\partial}{\partial z}T(z,t)\right) + Q \\ \dfrac{\partial c(r_c,z,t)}{\partial t} = \dfrac{1}{r_c}\dfrac{\partial}{\partial r_c}\left(D\left(T(z,t),\dot{F}\right)r\dfrac{\partial}{\partial r_c}c(r_c,z,t)\right) + \dfrac{\partial}{\partial z}\left(D\left(T(z,t),\dot{F}\right)\dfrac{\partial}{\partial z}c(r_c,z,t)\right) + S \end{cases} \tag{2}$$

where z (m) is the coordinate along the axis of the cylindrical grain i.e., along the radius of the pellet, r_c is the radial coordinate within the cylindrical grain, α (m^2 s^{-1}) is the thermal diffusivity, Q (K s^{-1}) is the heat

[1] In the application to fission gas models, the quasi-stationary approach proposed by Speight [39] is also adopted. It consists in lumping the diffusion towards the grain boundaries, the trapping rate g and the resolution rate b of atoms in/from intra-granular bubbles into an effective diffusion coefficient $D_{\text{eff}}\left(\text{m}^2\ \text{s}^{-1}\right)$:$D_{\text{eff}} = \frac{b}{b+g}D$restating the mathematical problem as purely diffusive, with $b/(b+g)$ called the quasi-stationary term. The intra-granular diffusion problem becomes$\frac{\partial c_t(r_s,t)}{\partial t} = D_{\text{eff}}\frac{1}{r_s^2}\frac{\partial}{\partial r_s}\left(r_s^2\frac{\partial}{\partial r_s}c_t(r_s,t)\right) + S$where $c_t\left(\text{at m}^{-3}\right)$ is the total intra-granular gas concentration considering both the concentration of single gas atoms dissolved in the lattice and the concentration of gas atoms in intra-granular bubbles. For the purposes of this work, which is the development and verification of the reduced order model describing the diffusion process, this equation is formally identical to Eq. (1).

generation rate.

Let us consider these two diffusion problems (Eq. (1) and (2)) under constant conditions (i.e., the diffusion coefficient related to the spherical case D, the gas source term S and the heat source term Q are assumed to be constant in time and uniform in space). Each individual grain is assumed to have a grain-boundary surface that acts as a "perfect sink". This defines a mathematical boundary condition of a zero gas concentration immediately adjacent to the grain boundary, i.e., $c(R_s,t)=0$, $c(r_c,L,t)=0$, $c(R_c,z,t)=0$ and $c(r_c,0,t)=0$ for $t>0$, $R_c \geqslant r_c \geqslant 0$ and $L \geqslant z \geqslant 0$ with R_s(m), R_c(m) and L(m) being the radii of the spherical and cylindrical grain, and the length of the cylindrical grain, respectively. As initial condition ($t=0$) we consider both $c(r_s,t)=0$ and $c(r_c,z,t)=0$. Consequently, in the spherical symmetry case, the concentration field satisfies the system of equations:

$$\begin{cases} \dfrac{\partial c(r_s,t)}{\partial t} = D(T,\dot{F})\dfrac{1}{r_s^2}\dfrac{\partial}{\partial r_s}\left(r_s^2\dfrac{\partial}{\partial r_s}c(r_s,t)\right)+S & \\ c(r_s,0)=0 & R_s \geqslant r_s \geqslant 0 \\ c(R_s,t)=0 & t>0 \end{cases} \tag{3}$$

while, when the cylindrical symmetry is considered, it solves the problem:

$$\begin{cases} \dfrac{\partial c(r_c,z,t)}{\partial t} = \dfrac{1}{r_c}\dfrac{\partial}{\partial r_c}\left(D\left(T(z,t),\dot{F}\right)r\dfrac{\partial}{\partial r_c}c(r_c,z,t)\right)+\dfrac{\partial}{\partial z}\left(D\left(T(z,t),\dot{F}\right)\dfrac{\partial}{\partial z}c(r_c,z,t)\right)+S & \\ c(r_c,z,0)=0 & R_c \geqslant r_c \geqslant 0, L \geqslant z \geqslant 0 \\ c(r_c,L,t)=0 & R_c \geqslant r_c \geqslant 0, t>0 \\ c(R_c,z,t)=0 & L \geqslant z \geqslant 0, t>0 \\ c(r_c,0,t)=0 & R_c \geqslant r_c \geqslant 0, t>0 \end{cases} \tag{4}$$

For what concerns the temperature problem we consider as initial condition $T(z,0)=2000$ K (as a representative value, without lack of generality), a Dirichlet boundary condition of $T(z,t)=2000$ K on one of the cylinder bases, γ_1, and a null Neumann boundary condition on the other base (corresponding to the interface with the pellet central void), γ_2, and on the lateral surface, γ_3 (Fig. 1b). Consequently $T(z,t)$ satisfy the following problem:

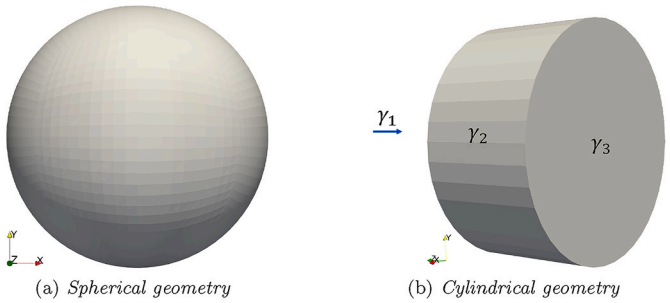

(a) *Spherical geometry* (b) *Cylindrical geometry*

Fig. 1. Geometry used for the full order simulation implemented in OpenFOAM. γ_3 represents the surface closest to the center of the pellet while γ_1 the furthest surface, γ_2 is the lateral surface of the cylindrical grains.

$$\begin{cases} \dfrac{\partial T(z,t)}{\partial t} = \alpha\dfrac{\partial}{\partial z}\left(\dfrac{\partial}{\partial z}T(z,t)\right)+Q & \\ T(z,0)=2000\ \text{K} & L \geqslant z \geqslant 0 \\ T(z,t)=2000\ \text{K} & \text{on}\ \ z=L, t>0 \\ \dfrac{\partial T(z,t)}{\partial z}=0 & \text{on}\ \ R_c \geqslant r_c \geqslant 0 \text{ or } z=0, t>0 \end{cases} \tag{5}$$

For the purpose of modelling intra-granular fission gas diffusion in fuel performance codes, the engineering figure of merit is the weighted volume average in the grain of the total gas concentration along time, i.e., $\overline{c}(t)=\frac{1}{V}\int c(t)\ \mathrm{d}V$ with V the volume of the grain.

Eqs. (3)–(5) represent a mathematical model describing intra-granular fission gas behaviour in restructured oxide fuel in fast reactor conditions. Such model is not exhaustive on its own and requires to be paired with a consistent model for the inter-granular behaviour and with a dedicated model for the high burnup structure [40]. Nevertheless, the treatment of intra-granular diffusion is the first and fundamental step in the modelling process. Its numerical solution is thus presented in the following section.

It is worth noting that Eqs. (3)–(5) require particular care to be included in the frame of fuel performance codes (whereas similar descriptions for oxide fuel in light water reactor conditions are generally applicable, e.g., Refs. [6,32,41–43]). This is due to the size of columnar grains (range of hundreds of microns up to a millimeter) which exceeds the typical size of mesh cell used in fuel performance simulations, contrary to the size of unrestructured spherical grains (few microns). For this reason, it is not possible to invoke this model in each mesh element/quadrature point, requiring a dedicated interface between the grain-scale model and the rest of fuel performance pellet-scale models.

3. Full order model

Eqs. (3)–(5) with their respective boundary conditions has been implemented in OpenFOAM [44] in order to compute the so called *snapshots* [30] i.e., the solutions of the diffusion problem at different time steps, that will be used to build the basis functions (Section 5). To simplify implementation and without loss of generality, a dimensionless geometry has been adopted (Fig. 1). For the case of spherical domain, Eq. (1) have been transformed into a dimensionless form:

$$R_s^2\frac{\partial c}{\partial t} = D\frac{1}{\rho_s^2}\frac{\partial}{\partial \rho_s}\left(\rho_s^2\frac{\partial}{\partial \rho_s}c\right)+R_s^2 S \tag{6}$$

where $\rho_s = r_s/R_s$. Simplifying the notation of the dimensionless Laplacian operator we obtain:

$$R_s^2\frac{\partial c}{\partial t} = D\nabla^2 c + R_s^2 S \tag{7}$$

Table 1
Values and u.o.m of the parameters adopted in the simulation of fission gas diffusion, in spherical and cylindrical grains.

Symbol	Parameter	Value		u.o.m
		Sphere	Cylinder	
c	Concentration			mol m^{-3}
T	Temperature	1200		K
R_s	Spherical grain radius	5×10^{-6}		m
R_c	Cylindrical grain radius		1×10^{-5}	m
L	Grain length		1×10^{-3}	m
$\dot{F}$	Fission rate density	3×10^{19}	3×10^{19}	fiss m^{-3} s^{-1}
D	Diffusion coefficient	$D_1 + D_2 + D_3$ [45,46] $D_1 = 7.6 \times 10^{-10} \exp(-4.86 \times 10^{-19}/k_B T)$ $D_2 = 5.64 \times 10^{-25} \sqrt{\dot{F}} \exp(-1.91 \times 10^{-19}/k_B T)$ $D_3 = 2 \times 10^{-40} \dot{F}$		m^2 s^{-1}
		k_B (J K^{-1}), Boltzmann constant		
α	Thermal diffusivity		5×10^{-7}	m^2 s^{-1}
S	Gas source	1.5×10^{-5}	1.5×10^{-5}	mol m^{-3}s^{-1}
Q	Heat source		218.1	K s^{-1}

The use of dimensionless coordinates allows adopting a spherical mesh of unitary radius (Fig. 1a) and to introduce the grain radius directly in the equation parameters.

For the case of cylindrical domain, the spatial dimensionless form of Eq. (2) turns out to be:

$$\begin{cases} L^2 \dfrac{\partial}{\partial t} T - \alpha \dfrac{\partial}{\partial \xi} \left(\dfrac{\partial}{\partial \xi} T \right) = L^2 Q \\ \dfrac{\partial}{\partial t} c - \dfrac{1}{R_c^2} \dfrac{1}{\rho_c} \dfrac{\partial}{\partial \rho_c} \left(D(T(\xi)) \rho_c \dfrac{\partial}{\partial \rho_c} c \right) - \dfrac{1}{L^2} \dfrac{\partial}{\partial \xi} \left(D(T(\xi)) \dfrac{\partial}{\partial \xi} c \right) = S \end{cases} \tag{8}$$

where $\rho_c = r_c/R_c$ and $\xi = z/L$. The anisotropy of the cylindrical diffusion problem has been treated through the tensor representation of the diffusion coefficient. In particular, the x and y components have been divided by the squared length of the radius while the z component by the squared length of the height of the cylinder. Compacting Eq. (8) and introducing the tensorial diffusion coefficient:

$$\begin{cases} L^2 \dfrac{\partial T}{\partial t} = \alpha \nabla^2 T + L^2 Q \\ \dfrac{\partial c}{\partial t} = \dfrac{D}{R_c^2} \nabla \cdot (\mathbf{G} \nabla c) + S \end{cases} \tag{9}$$

where:

$$\mathbf{D} = \frac{D}{R_c^2} \begin{bmatrix} 1 & 0 & 0 \\ 0 & 1 & 0 \\ 0 & 0 & \dfrac{R_c^2}{L^2} \end{bmatrix} = \frac{D}{R_c^2} \mathbf{G} \tag{10}$$

In this case the dimensionless notation allows adopting a cylindrical mesh of unitary radius and unitary length (Fig. 1b). Then we introduce the radius and the length of the cylindrical grain directly as parameters in the equation and we treat the anisotropy of the problem in the tensor **G**.

The parameters adopted for the simulations are collected in Table 1. The two simulations of diffusion in the spherical geometry and in the cylindrical geometry are run respectively for 7.5×10^8 s and for 1×10^7 s. These times were chosen on the basis of the relaxation time, i.e., the time taken by the phenomena to reach equilibrium, and were calculated by dividing the square radius of the grain by the diffusion coefficient. Meshes with 80′000 cells are adopted for the spherical and cylindrical geometry. Figure (2) depicts the distribution of concentration field for different time steps resulting from the full-order spherical model implemented in OpenFOAM. Given the isotropic diffusion and the symmetrical geometry and mesh, we obtain a symmetrical distribution that at equilibrium assumes a parabolic trend along the spatial coordinates. In Fig. (3), is depicted the concentration and temperature fields for different time steps resulting from the full-order cylindrical model implemented in OpenFOAM. In this case, the direction of greatest interest to be analyzed is the z direction of the columnar grains corresponding to the direction along the fuel pellet radius and along which the steep temperature gradient is established. The diffusion coefficient is higher in the inner part of the pellet, where the temperature is higher and decreases moving outside. This creates a concentration gradient along the z axis of the columnar grain opposite to the temperature gradient and consequently a flux of gas moving towards the hotter part of the grain. This transport of gas implies a higher release since it is directed towards the part of the columnar grain with higher diffusivity.

A verification in terms of exact solutions is carried out on the weighted volume average concentration. For the case of spherical diffusion, the weighted volume average concentration computed with OpenFOAM reaches the correct analytical asymptotic value [15,20], with a relative error of 0.48%.

4. Reduced order model

In this section, the goal is to present the procedure to obtain a POD-Galerkin ROM (POD-G-ROM) of Eqs. (7) and (8), considering the Finite Volume approximation (POD-FV-ROM) [47]. The procedure here described is applicable to both the spherical and cylindrical geometry. The main assumption in the reduced order techniques based on projection method is that the approximated solution of the problem $c_r(\mathbf{x}, t)$ can be expressed as linear combination of the spatial modes $\varphi_i(\mathbf{x})$ multiplied by the temporal coefficients $a_i(t)$. Therefore, the first step consists in the expansion of the field in the series of orthonormal spatial modes:

$$c(\mathbf{x}, t) \approx c_r(\mathbf{x}, t) = \sum_{i=1}^{N_c} a_i(t) \varphi_i(\mathbf{x}) \tag{11}$$

where N_c is the number of modes adopted for the concentration field. For the diffusion in cylindrical grains it is also necessary to expand the temperature field:

$$T(\mathbf{x}, t) \approx T_r(\mathbf{x}, t) = \sum_{i=1}^{N_T} b_i(t) \varphi_i(\mathbf{x}) \tag{12}$$

where N_T is the number of modes adopted for the temperature field.

In this work, the POD procedure is adopted thanks to its capability to select the most energetic modes, i.e., the modes representing the most significant features of the problem. This results into a very cost-effective solution retaining all the fundamental information of the model, while reducing its complexity. The set of spatial modes is built starting from the *snapshots*, i.e., the values of the fields $c(\mathbf{x}, t)$ and $T(\mathbf{x}, t)$ at prescribed times t_n for $n = 1, \ldots, N_s$, i.e., $c_n = c(\mathbf{x}, t_n)$ and $T_n = T(\mathbf{x}, t_n)$, where N_s is the number of snapshots adopted. In the simulation of the spherical and cylindrical case, the frequency of snapshot sampling was set to 1.333×10^{-6} Hz and 1×10^{-4} Hz respectively, in order to collect 1000 snapshots during the 7.5×10^8 and 1×10^7 s of simulation.[2] The spatial set of modes is built minimizing the L^2-norm of the least square difference between the snapshots and the projection of the snapshots in the subspaces $X_c^{\mathrm{POD}} = \mathrm{span}\{\varphi_1, \varphi_2, \ldots, \varphi_{N_c}\}$ and $X_T^{\mathrm{POD}} = \mathrm{span}\{\varphi_1, \varphi_2, \ldots, \varphi_{N_T}\}$, paired with the orthonormality of the modes [47]:

[2] The computational time required by a Intel Core i5-5300U CPU @ 2.30 GHz and 8 GB RAM was in the order of 5 min and 10 min for the simulations, respectively.

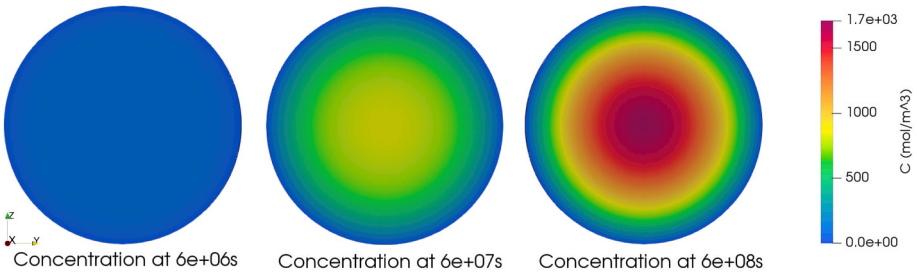

Fig. 2. The concentration distributions in the spherical fuel grain with respect to three time steps resulting from the full order simulation implemented in OpenFOAM. The concentration field reaches the asymptotic value at 6×10^8 s.

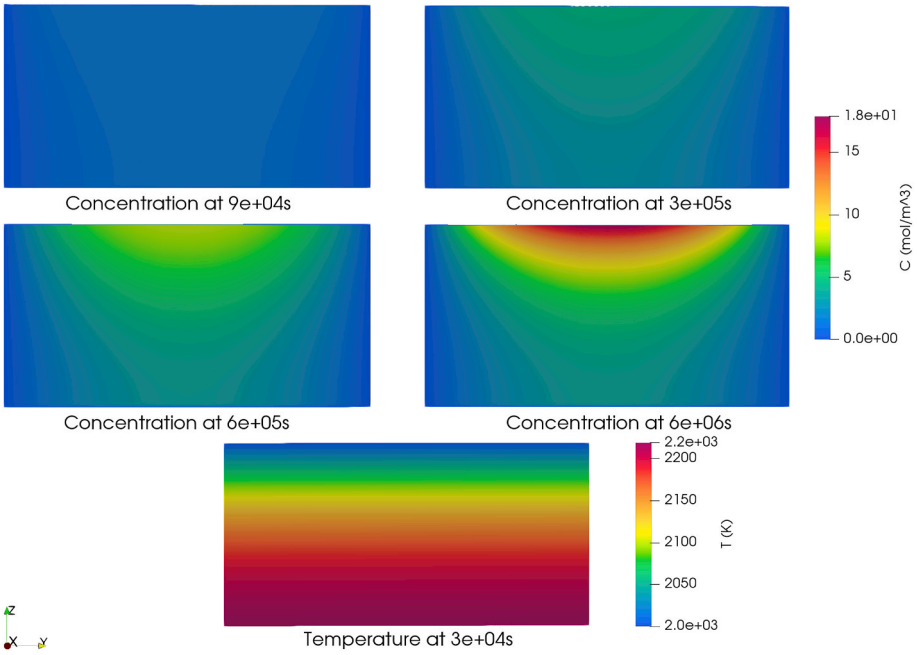

Fig. 3. The concentration and temperature distributions in the cylindrical fuel grain with respect to four time steps resulting from the full order simulation implemented in OpenFOAM. The concentration field reaches the asymptotic value at 6×10^6 s, instead, the temperature field reaches it rapidly already at 3×10^4 s. The top of the rectangle corresponds to the surface γ_1.

$$X_c^{\mathrm{POD}} = \arg\min \frac{1}{N_s} \sum_{n=1}^{N_s} \| c_n - \sum_{i=1}^{N_c} \langle c_n, \phi_i(\mathbf{x}) \rangle \phi_i(\mathbf{x}) \|_{\mathrm{L}^2}^2, \text{constrained by} \langle \phi_i(\mathbf{x}), \phi_j(\mathbf{x}) \rangle_{\mathrm{L}^2} = \delta_{ij} \tag{13}$$

$$X_T^{\mathrm{POD}} = \arg\min \frac{1}{N_s} \sum_{n=1}^{N_s} \| T_n - \sum_{i=1}^{N_T} \langle T_n, \varphi_i(\mathbf{x}) \rangle \varphi_i(\mathbf{x}) \|_{\mathrm{L}^2}^2, \text{constrained by} \langle \varphi_i(\mathbf{x}), \varphi_j(\mathbf{x}) \rangle_{\mathrm{L}^2} = \delta_{ij} \tag{14}$$

where δ_{ij} is the Kronecker delta. Eqs. (13) and (14) are solved by introducing suitable correlation matrices according to the procedure reported in Refs. [28,47], formally solving an eigenvalue-eigenvector problem for both concentration and temperature:

$$E\boldsymbol{\xi}_i = e_i \boldsymbol{\xi}_i \quad i = 1, \ldots, N_s \tag{15}$$

$$K\boldsymbol{\chi}_j = k_j \boldsymbol{\chi}_j \quad j = 1, \ldots, N_s \tag{16}$$

where e_i and k_j are the eigenvelues, $\boldsymbol{\xi}_i$ and $\boldsymbol{\chi}_j$ are the eigenvectors, and $E \in \mathbb{R}^{N_s \times N_s}$ and $K \in \mathbb{R}^{N_s \times N_s}$ are the correlation matrices. The $(e_i, \boldsymbol{\xi}_i)$ and $\left(k_j, \boldsymbol{\chi}_j\right)$ eigenvalue–eigenvector pairs are used to build the spatial modes as:

$$\varphi_i(\mathbf{x}) = \frac{1}{\sqrt{e_i}} \sum_{n=1}^{N_s} \xi_{i,n} c_n(\mathbf{x}) \quad i = 1, \ldots, N_c \tag{17}$$

$$\varphi_i(\mathbf{x}) = \frac{1}{\sqrt{k_i}} \sum_{n=1}^{N_s} \chi_{i,n} T_n(\mathbf{x}) \quad i = 1, \ldots, N_T \tag{18}$$

Since the eigenvalues are sorted in descending order, the first modes are those retaining most of the energy of the complete solution [48]. This ensures that however the series in Eqs. (11) and (12) are truncated, the most energetic modes are saved.

4.1. Spherical grain

Concerning the spherical grain case, replacing the concentration c with c_r (Eq. (11)) in Eq. (7), we obtain:

$$R_s^2 \sum_{i=1}^{N_c} \varphi_i(\mathbf{x}) \frac{\partial a_i(t)}{\partial t} = D \sum_{i=1}^{N_c} \left(a_i(t) \nabla^2 \varphi_i(\mathbf{x}) \right) + R_s^2 S \tag{19}$$

Applying the Galerkin projection over the test functions $\varphi_j(\mathbf{x})$ and exploiting the orthonormality of the modes with respect to the L^2 inner product:

$$R_s^2 \frac{\mathrm{d}a_j(t)}{\mathrm{d}t} = D \sum_{i=1}^{N_c} a_i(t) \int_{\Omega_s} \varphi_j(\mathbf{x}) \nabla^2 \varphi_i(\mathbf{x}) \mathrm{d}\Omega_s + R_s^2 S \int_{\Omega_s} \varphi_j(\mathbf{x}) \mathrm{d}\Omega_s \quad j = 1, \ldots, N_c \tag{20}$$

where Ω_s is the volume of the sphere. By introducing A_{ji} and B_j, the following POD-Galerkin ROM (POD-G-ROM) for Finite Volume discretization (POD-FV-ROM) is obtained:

$$\frac{\mathrm{d}a_j(t)}{\mathrm{d}t} = \frac{D}{R_s^2} \sum_{i=1}^{N_c} a_i(t) A_{ji} + S B_j \quad j = 1, \ldots, N_C \tag{21}$$

with $A_{ji} = \langle \varphi_j(\mathbf{x}), \nabla^2 \varphi_i(\mathbf{x}) \rangle_{\mathrm{L}^2}$ and $B_j = \langle \varphi_j(\mathbf{x}) \rangle_{\mathrm{L}^2}$.

4.2. Cylindrical grain

For the cylindrical grain case, we start by considering the temperature equation. The boundary conditions are enforced explicitly through the use of the penalty method [49]. Given γ_1 the portion of the domain on which the Dirichlet boundary condition is applied to the temperature ($T_{\mathrm{BC}} = 2000$ K, Fig. 1bb):

$$T(\mathbf{x} \in \gamma_1, t) = T_{\mathbf{BC}} \tag{22}$$

Introducing the penalty factor τ_T, the boundary condition T_{BC} in the first equation of the System (9) is enforced as follows:

$$L^2 \frac{\partial T(\mathbf{x}, t)}{\partial t} = \alpha \nabla^2 T(\mathbf{x}, t) + L^2 Q + \tau_T (T(z) - T_{BC}(z)) (\delta(z - 0) + \delta(z - L)) \tag{23}$$

Replacing the temperature T with T_r (Eq. (12)), performing the Galerkin projection over the test functions $\varphi_j(\mathbf{x})$ and exploiting the orthonormality of the modes with respect to the L^2 inner product:

$$L^2 \frac{\mathrm{d}b_j(t)}{\mathrm{d}t} = \alpha \sum_{n=1}^{N_T} b_i(t) \int_{\Omega_c} \varphi_j(\mathbf{x}) \cdot \nabla^2 \varphi_i(\mathbf{x}) \mathrm{d}\Omega_c + L^2 Q \int_{\Omega_c} \varphi_j(\mathbf{x}) \mathrm{d}\Omega_c - \tau_T \int_{\gamma_1} \varphi_j(\mathbf{x}) \left(T_{\mathrm{BC}} - \sum_{i=1}^{N_T} b_i(t) \varphi_i(\mathbf{x}) \right) \mathrm{d}\gamma_1 \quad j = 1, \ldots, N_T \tag{24}$$

where Ω_c is the volume of the cylinder. Rewriting Eq. (24) in matrix terms, the POD-G-ROM for finite volume discretization is:

$$\frac{\mathrm{d}b_j(t)}{\mathrm{d}t} = \frac{\alpha}{L^2} \sum_{n=1}^{N_T} b_i(t) H_{ji} + Q L_j + \frac{\tau_T}{L^2} \sum_{i=1}^{N_T} J_{ji} b_i(t) - \frac{\tau_T T_{\mathrm{BC}}}{L^2} K_j \quad j = 1, \ldots, N_T \tag{25}$$

with $H_{ji} = \langle \varphi_j(\mathbf{x}), \nabla^2 \varphi_i(\mathbf{x}) \rangle_{\mathrm{L}^2}$, $L_j = \langle \varphi_j(\mathbf{x}) \rangle_{\mathrm{L}^2}$, $J_{ji} = \langle \varphi_j(\mathbf{x}), \varphi_i(\mathbf{x}) \rangle_{\mathrm{L}^2, \gamma_1}$, and $K_j = \langle \varphi_j(\mathbf{x}) \rangle_{\mathrm{L}^2, \gamma_1}$.

As for the concentration, replacing c with c_r (Eq. (11)) in Eq. (9) we obtain:

$$\sum_{i=1}^{N_C} \varphi_i(\mathbf{x}) \frac{\partial a_i(t)}{\partial t} = D \frac{1}{R_c^2} \nabla \cdot \left(\mathbf{G} \cdot \sum_{i=1}^{N_C} \nabla (a_i(t) \varphi_i(\mathbf{x})) \right) + S \tag{26}$$

In this case, diversely from the spherical grain in which the temperature and hence the diffusivity are assumed uniform within the domain, the relationship between the diffusion coefficient and the temperature field is not affine, i.e., the diffusion coefficient cannot be written as a linear combination of the temperature, therefore the dependence on temperature by the diffusion coefficient has been modeled by means of a linear relation:

$$D = D^0 + \alpha^D (T - T^0) \tag{27}$$

where D^0, T^0 and α^D are constant values. D^0 is the diffusion coefficient in correspondence of T^0 and α^D is equal to the partial derivative of diffusion coefficient with respect to temperature obtained in correspondence of T^0. The linearized approach allows to have an affine decomposition with respect to temperature. Replacing the temperature T with T_r (Eq. (12)), applying the Galerkin projection over the test functions $\varphi_j(\mathbf{x})$ and rewriting the equation in matrix terms, the following POD-FV-ROM is obtained:

$$\frac{\mathrm{d}a_j(t)}{\mathrm{d}t} = \frac{1}{R_c^2} \left(D^0 - \alpha^D T^0 \right) \sum_{i=1}^{N_C} a_i(t) X_{ji} + \frac{1}{R_c^2} \alpha^D \sum_{k=1}^{N_T} \sum_{i=1}^{N_C} b_k(t) a_i(t) M_{jki} + + \frac{1}{R_c^2} \alpha^D \sum_{k=1}^{N_T} \sum_{i=1}^{N_C} b_k(t) a_i(t) N_{jki} + S P_j \quad j = 1, \ldots, N_c \tag{28}$$

with $X_{ji} = \langle \varphi_j(\mathbf{x}), \nabla \cdot (\mathbf{G} \nabla \varphi_i(\mathbf{x})) \rangle_{\mathrm{L}^2}$, $M_{jki} = \langle \varphi_j(\mathbf{x}), \langle \varphi_k(\mathbf{x}), \nabla \cdot (\mathbf{G} \nabla \varphi_i(\mathbf{x})) \rangle \rangle_{\mathrm{L}^2}$, $N_{jki} = \langle \varphi_j(\mathbf{x}), \langle \nabla \varphi_k(\mathbf{x}), \mathbf{G} \nabla \varphi_i(\mathbf{x}) \rangle \rangle_{\mathrm{L}^2}$, and $P_j = \langle \varphi_j(\mathbf{x}) \rangle_{\mathrm{L}^2}$.

4.3. Summary

With this procedure, the original PDEs systems (Eq. (1) and (2)) are replaced by ODEs systems (Eq. (21), (25) and (28)) in which the unknowns are the time-dependent coefficients $a_i(t)$ and $b_i(t)$. The ODEs systems for the spherical and cylindrical geometry can be expressed respectively as the following dynamical systems, for the spherical grain case:

$$\dot{\mathbf{a}} = \frac{D}{R_s^2} \mathbf{a} \mathbf{A} + S \mathbf{B} \tag{29}$$

and for the cylindrical grain case:

$$\dot{\mathbf{b}} = \frac{\alpha}{L^2} \mathbf{b} \mathbf{H} + Q \mathbf{L} + \tau_T \left(\frac{1}{L^2} \mathbf{J} \mathbf{b} - \frac{T_{\mathrm{BC}}}{L^2} \mathbf{K} \right) \tag{30}$$

$$\dot{\mathbf{a}} = \frac{1}{R_c^2} \left(D^0 - \alpha^D T^0 \right) \mathbf{a} \mathbf{X} + \frac{1}{R_c^2} \alpha^D \dot{\mathbf{b}} \mathbf{a} \mathbf{M} + \frac{1}{R_c^2} \alpha^D \dot{\mathbf{b}} \mathbf{a} \mathbf{N} + S \mathbf{P} \tag{31}$$

where the apex indicates the transposition of the vector and the dot refers to the time derivative. Despite the unknowns $a_i(t)$ and $b_i(t)$ depend exclusively on time, the systems also provides a spatial description, since the spatial character is included in the matrices that have been

Table 2
Eigenvalues of the concentration and temperature fields in the spherical and cylindrical cases with respect to the number of modes adopted.

Index	Spherical case	Cylindrical case	
	Concentration eigenvalue	Concentration eigenvalue	Temperature eigenvalue
1	2.44×10^{9}	6.07×10^{4}	1.44×10^{10}
2	9.54×10^{5}	128	5.55×10^{-5}
3	7.43×10^{3}	4.02	1.29×10^{-5}
4	183	0.320	4.93×10^{-5}
5	8.12	0.040	3.08×10^{-6}
6	0.585	0.004	2.09×10^{-6}
7	0.130	7.63×10^{-4}	1.25×10^{-6}
8	0.020	1.34×10^{-4}	8.15×10^{-7}
9	0.015	2.95×10^{-5}	6.33×10^{-7}
10	0.002	1.04×10^{-5}	5.31×10^{-7}

calculated with the orthonormal modes. The construction of the matrix of Eqs. (29)–(31), which represent the last step of the Offline procedure, is performed in OpenFOAM.

5. Online procedure and numerical verification

The inexpensive Online computational step, i.e., the ODEs systems solving, is performed in the 0-D open-source computer code SCIANTIX [32,33] by means of an Implicit Euler scheme in order to derive the time coefficients and finally reconstruct the solution. SCIANTIX is a meso-scale module able to cover the description of intra- and inter-granular inert gas behaviour in nuclear fuels (e.g., UO_2 or MOX fuel) and has been designed to be coupled in existing fuel performance codes. The implementation in SCIANTIX allows comparing the reduced order model related to the spherical case with the state-of-the-art algorithms to verify its performances (Section 6). The implicit numerical scheme adopted to solve Eqs. (29)–(31) is based on the backward Euler method:

$$\mathbf{a}^{j+1} = \left(I - \frac{D}{R_s^2}\Delta t\mathbf{A}\right)^{-1}\left(\mathbf{a}^{j} + S\Delta t\right) \tag{32}$$

$$\mathbf{b}^{j+1} = \left(I - \frac{\alpha}{L^2}\Delta t\mathbf{H} - \frac{\tau_T}{L^2}\Delta t\mathbf{J}\right)^{-1}\left(\mathbf{b}^{j} + Q\Delta t\mathbf{L} - \frac{\tau_T T_{\mathrm{BC}}}{L^2}\Delta t\mathbf{K}\right) \tag{33}$$

$$\mathbf{a}^{j+1} = \left(I - \frac{1}{R_c^2}\Delta t\left(D^0 - \alpha^D T^0\right)\mathbf{X} - \frac{1}{R_c^2}\alpha^D\Delta t\left(\mathbf{b}^{j}\right)'\mathbf{M} - \frac{1}{R_c^2}\alpha^D\Delta t\left(\mathbf{b}^{j}\right)'\mathbf{N}\right)^{-1}\left(\mathbf{a}^{j} + S\Delta t\mathbf{P}\right) \tag{34}$$

where j is the time-step index and Δt is the time step. For T^0 we have adopted the volume-weighted average temperature and through a sensitivity analysis on the penalty factor we selected $\tau_T = 1$. At each time step, the code solves these ODEs for the time coefficients $\mathbf{a}^{j+1}$ and $\mathbf{b}^{j+1}$.

For the purpose of modelling intra-granular fission gas release, the engineering figure of merit is the average concentration. Therefore, the time coefficients calculated, $\mathbf{a}^{j+1}$ and $\mathbf{b}^{j+1}$, are multiplied by the volume-weighted average of the modes in order to obtain the volume-weighted average concentration:

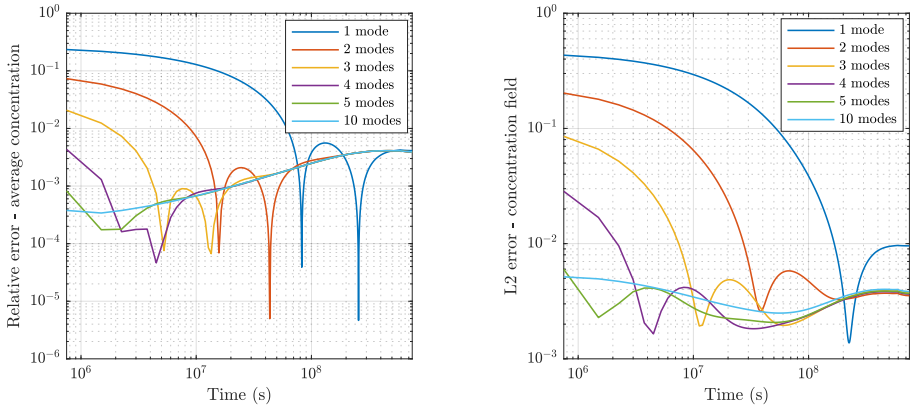

(a) Average concentration reconstructed in SCIANTIX (b) Concentration field reconstructed in OpenFOAM

Fig. 4. Errors of the reconstructed concentration from the ROM model of the spherical case with increasing the number of modes.

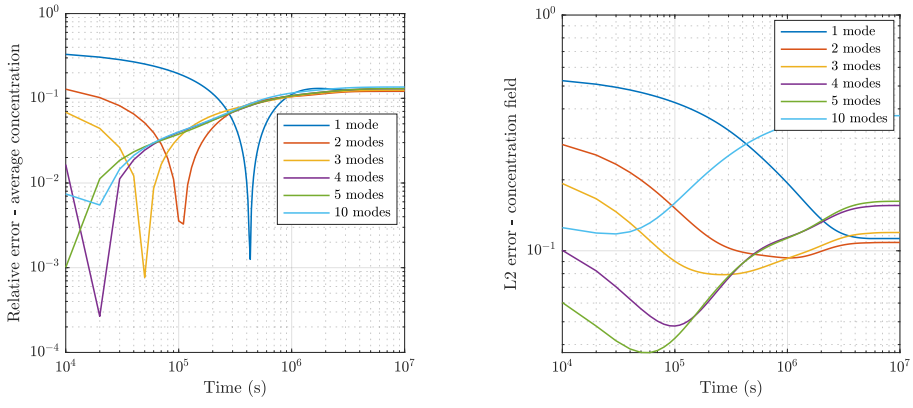

(a) Average concentration reconstructed in SCIANTIX (b) Concentration field reconstructed in OpenFOAM

Fig. 5. Errors of the reconstructed concentration from the ROM model of the cylindrical case with increasing the number of modes. These values has been obtained using one single mode for the temperature field.

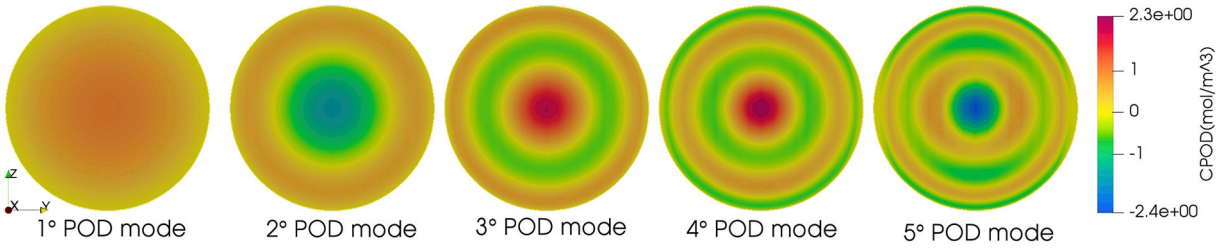

Fig. 6. The POD modes for the concentration in the spherical grain case resulting from the POD-FV-ROM implementation in OpenFOAM. These modes are parameterized in terms of the geometrical domain and the operating conditions.

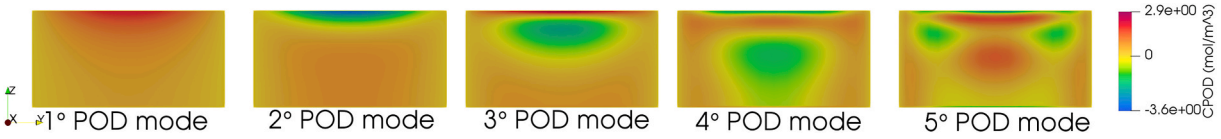

Fig. 7. The POD modes for the concentration in the cylindrical grain case resulting from the POD-FV-ROM implementation in OpenFOAM. These modes are parameterized in terms of the geometrical domain and the operating conditions.

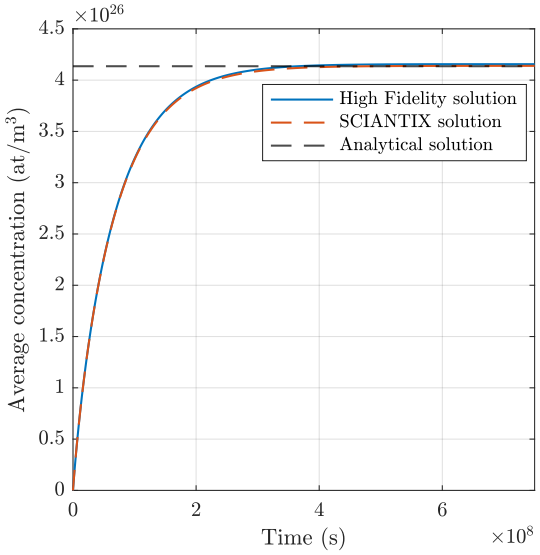

Fig. 8. Comparison between the SCIANTIX reconstruction, the high fidelity solution and the analytical solution at equilibrium of the spherical case in terms of average concentration.

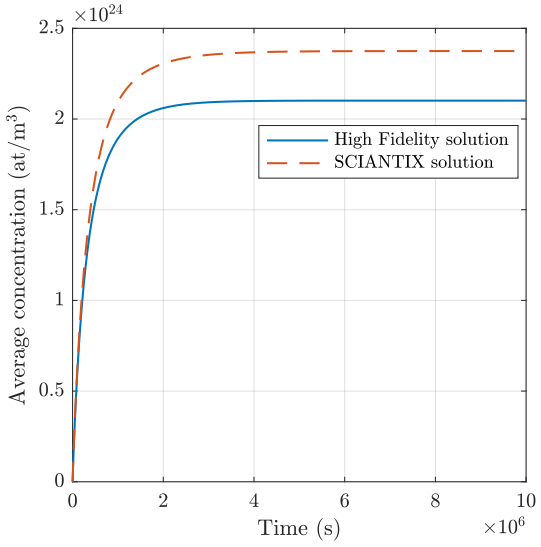

Fig. 9. Comparison between the SCIANTIX reconstruction and the high fidelity solution of the cylindrical case in terms of average concentration.

$$\overline{c}(\mathbf{x},t) = \sum_{i=1}^{N_c} a_i(t)\overline{\varphi}_i(\mathbf{x}) \tag{35}$$

The number of modes that should be adopted depends on the reducibility of the problem which can be evaluated by checking the decay of the eigenvalues of the correlation matrix. In Table 2, are reported the eigenvalues for the concentration and temperature fields respectively as a function of the number of modes. On the basis of these values, the concentration field, both for spherical and cylindrical cases, can be reconstructed with reasonable accuracy using five modes (the sixth accounts for 2.4 10^{-8}% of the sum of the first ten eigenvalues for the sphere case and 6.6 10^{-6}% for the cylinder case, respectively) instead for the temperature field one single mode is more than enough (second mode counting for 3.9 10^{-13}%). The same conclusions can be drawn by observing the errors reported in Figs. 4 and 5 for the spherical and cylindrical case, respectively. In Figs. 4a and 5a, are reported the relative errors over time obtained by comparing the average concentration of the FOM with respect the average concentration calculated in SCIANTIX, Eq. (35), as the number of modes varies. Instead Figs. 4b and 5b, as the number of modes varies shows the L^2 error between the concentration field of the FOM and the concentration field of the ROM model reconstructed in OpenFOAM through the temporal coefficient extracted from SCIANTIX. As can be seen, the most reasonable choice is to use five modes[3].

In Figs. 6 and 7, are reported the five modes for the spherical and cylindrical case, respectively. Through the use of these five modes, the average concentration over time reconstructed in SCIANTIX is compared with the average concentration of the FOM (i.e., the high-fidelity solutions presented in Section 3) in Figs. 8 and 9 for both cases. The maximum relative error between the high-fidelity solution and the reconstruction carried out in SCIANTIX is 0.41% for the spherical case and 13.01% for the cylindrical case. The higher error observed in the cylindrical case is not attributable to the geometry of the case. In fact,

[3] For the sphere case, it is worth noting that state-of-the-art algorithms available in fuel performance codes use expansions of the concentration solution with three to six terms, which is in line with what we obtained for the reduced order model.

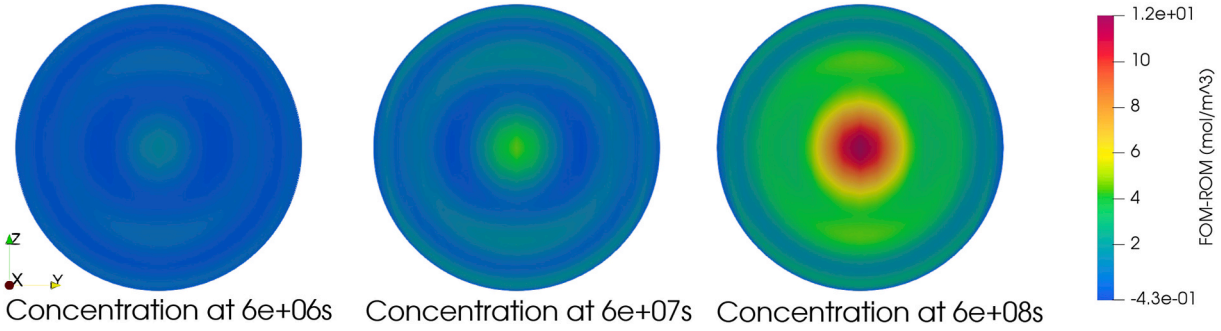

Fig. 10. Difference between the high fidelity concentration field and the reconstructed one for the spherical case in correspondence of three time steps.

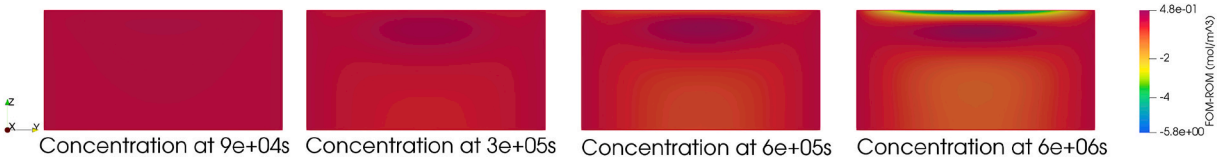

Fig. 11. Difference between the high fidelity concentration field and the reconstructed one for the cylindrical case in correspondence of three time steps.

the reconstruction of the concentration field with an imposed temperature, therefore without solving the heat equation as in the spherical case, returns a 1.4% error adopting five modes. Therefore, it is possible to conclude that this error is due to the linearization of the diffusion coefficient (Eq. (27)). This leaves room for future optimization of the proposed model using, e.g., a higher order approximation or a piecewise linear approximation of the diffusion coefficient.

The high error obtained for the cylindrical case is in line with the uncertainty analysis carried out in Ref. [50] from which is clear that the diffusion coefficient represent the parameter which dominates over the uncertainty associated with the asymptotic average concentration.

The difference of the spatial distribution of the concentration field between FOM and ROM, both for the spherical and cylindrical case, is reported in Figs. 10 and 11.

Summarizing, the application of the reduced order model for the spherical grain case requires: (i) once and for all the calculation of the matrices **A** and **B** which are then encoded in SCIANTIX; (ii) at each time step the five coupled ODEs (Eq. (32)) are solved; (iii) at each time step, Eq. (35) is used to reconstruct the solution. Similarly, the reduced order model for the cylindrical grain case requires: (i) once and for all the calculation of the matrices **H**, **J**, **K**, **L**, **X**, **M**, **N** and **P** which are then encoded in SCIANTIX; (ii) at each time step the four coupled ODEs (Eq. (33) and (34)) are solved; (iii) at each time step, Eq. (35) is used to reconstruct the solution in terms of average gas concentration.

6. Comparison with the state-of-the-art algorithms

In this Section we present a random numerical experiment aimed at comparing the accuracy and computational time of the reduced order model to other numerical algorithms for time-varying condition currently used in fuel performance codes. Since the proposed reduced order model for the cylindrical grain case is a first of a kind in the field of fuel performance, the comparison is dedicated to the spherical grain case, where comparison with the state-of-the-art is possible.

As comparisons, we selected the state-of-the-art FORMAS [13–15] algorithm and the quasi-exact ANS-5.4 algorithm [15–18]. In FORMAS the solution is obtained exploiting an expansion in a series of orthonormal eigenfunctions of the radial part of the spherical Laplacian. Among the various versions of the FORMAS algorithm, we adopt the one with four exponential terms [14], which is available in fuel performance codes, e.g. TRANSURANUS [9] and BISON [51]. This version of the FORMAS algorithm is thus solving four decoupled ODEs compared to the five coupled ODEs of the proposed algorithm. For what concerns the quasi-exact ANS-5.4 algorithm, it was used as a reference solution in several numerical experiments [15,20,52,53] because it is affected only by the numerical error due to discretization of a real operation history into piecewise-constant conditions. We adopt the ANS-5.4 algorithm with thirty spatial modes which guarantee excellent accuracy even in time-varying conditions.

6.1. Set-up of numerical experiment

Following the work of [20,21], the proposed numerical experiment consists of applying each algorithm to Eq. (1) for 1000 randomly-generated power histories. Each power history is piecewise-linear[4]. The following quantities are considered as random variables (sampled from uniform distributions):

- Number of linear steps [2;10];
- Time duration of each linear step [10 h; 10000 h];
- Temperature [1000 K; 3000 K];
- Fission rate [1×10^{18} fiss m^{-3}s^{-1}; 3×10^{19} fiss m^{-3}s^{-1}].

The conditions selected are such as to cover a fractional fission gas release (FGR) range of [0; 0.7]. The figure of merits for testing and comparing the algorithms are (i) the average concentration at the end of the history $\overline{c}_t(t_{\text{end}})$; (ii) the fractional FGR f at the end of the history; and (iii) the execution time t_{exe}[5]. The fractional FGR f is defined as:

$$f := \frac{\overline{c}_{\text{created}}(t_{\text{end}}) - \overline{c}_t(t_{\text{end}})}{\overline{c}_{\text{created}}(t_{\text{end}})} \tag{36}$$

where $\overline{c}_{\text{created}}$ is the concentration of gas created and t_{end} is the final time of the power history.

[4] The random histories of the numerical experiment reported in this Section have been constructed as piecewise-linear since this temporal discretization is typically applied in fuel performance codes.

[5] For this numerical experiment, we consider the mathematical formulation of the intra-granular fission gas release problem based on the hypothesis of equilibrium between bubble trapping and resolution (quasi-stationary approach). The models adopted for D_{eff}, b and g are [45,54,55], respectively. For the sake of the verification procedure, the choice of these models is not a strong requirement.

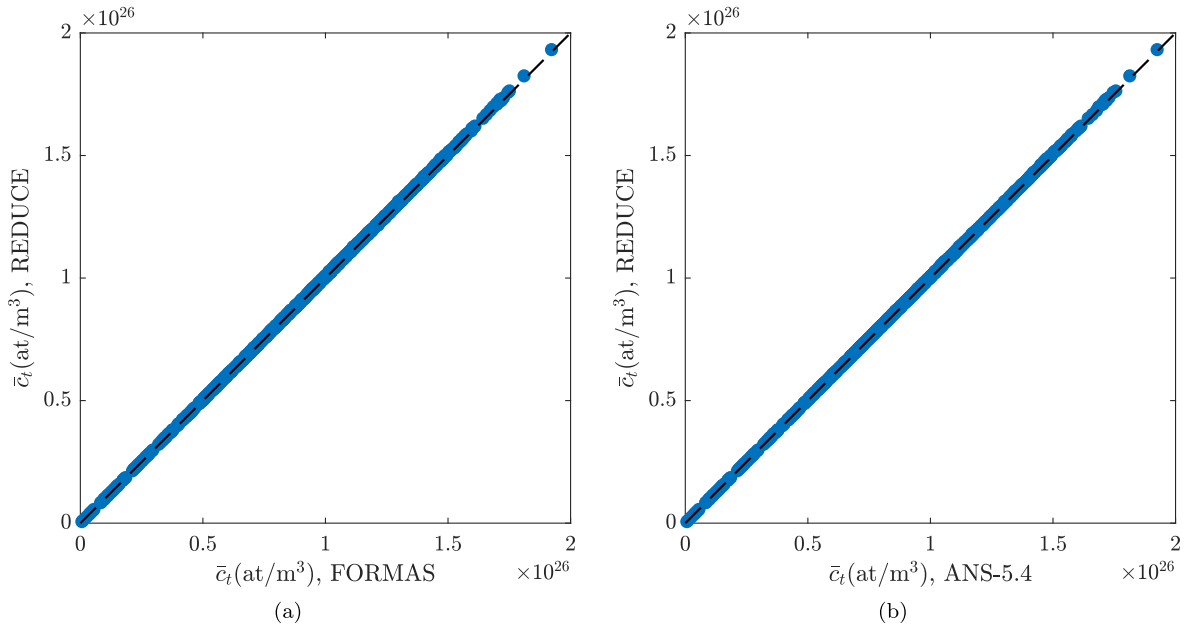

Fig. 12. Comparison between the values of intra-granular average fission gas concentration, $\bar{c}_t$, calculated by the REDUCE, FORMAS, and ANS-5.4 algorithms. Each point corresponds to a calculation with randomly generated conditions.

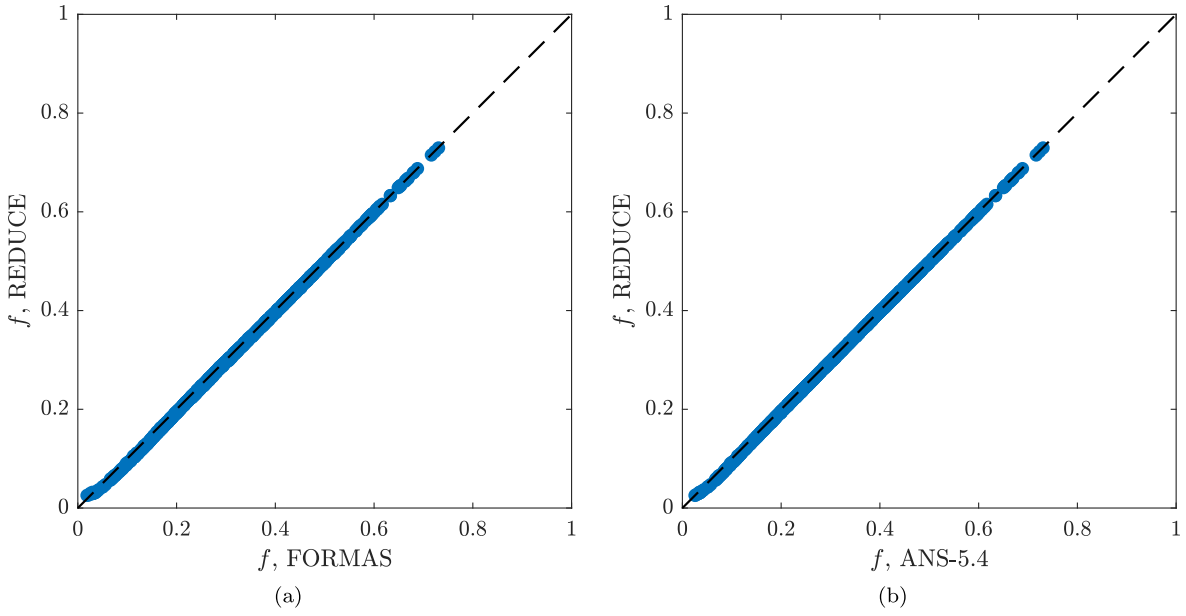

Fig. 13. Comparison between the values of intra-granular fission gas release calculated by the REDUCE, FORMAS, and ANS-5.4 algorithms. Each point corresponds to a calculation with randomly generated conditions.

6.2. Results and discussion

The results of the numerical experiment are presented in Figs. 12–14 for the FORMAS algorithm, the ANS-5.4 algorithm, and the reduced order algorithm applied to Eq. (1) (from here on referred to as REDUCE). Each point in these figures corresponds to one of 1000 randomly-generated power histories.

From Fig. 12, the deviation from the 45° diagonal is a measure of the accuracy. As can be seen, the REDUCE algorithm is able to calculate the intra-granular average concentration with a very good accuracy, indeed in the figures only a slight deviation is perceived corresponding to less than 1.3%. The reduced algorithm proves to be able to predict the solution also in correspondence of those stories characterized by steep variations of the parameters, although it has been implemented in constant conditions.

In Fig. 13, we have adopted the same graphic representation of the numerical experiment related to intra-granular average fission gas concentration. In this case, any deviation from the 45° is a measure of the accuracy in terms of intra-granular fission gas release. In the comparison figures, a deviation is perceived for release values lower than 0.2, where the REDUCE algorithm returns a slight underestimation. This behaviour is due to the fact that the FORMAS algorithm used in this work applies an artificial correction for $f < 0.1$ [15] which consists in approximating the solution with a polynomial term when $0 \leq f \leq 0.1$ with a relative error $< 10^{-6}$, while the ANS-5.4 algorithm computes a high-fidelity solution of the diffusion problem thanks to its

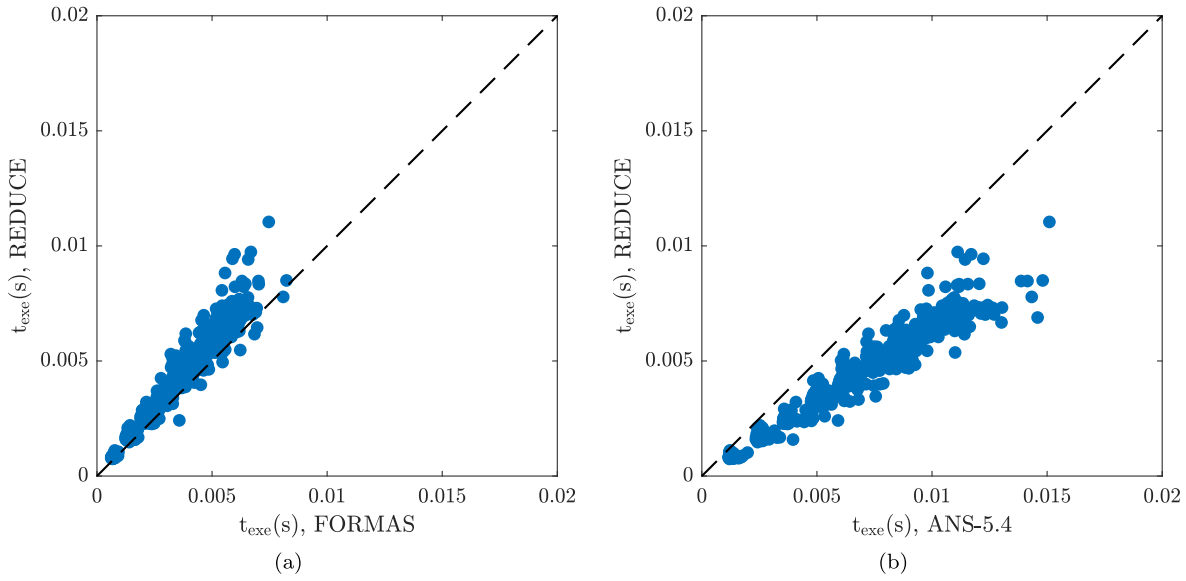

Fig. 14. Comparison between the values of execution time calculated by the REDUCE, FORMAS, and ANS-5.4 algorithms. Each point corresponds to a calculation with randomly generated conditions.

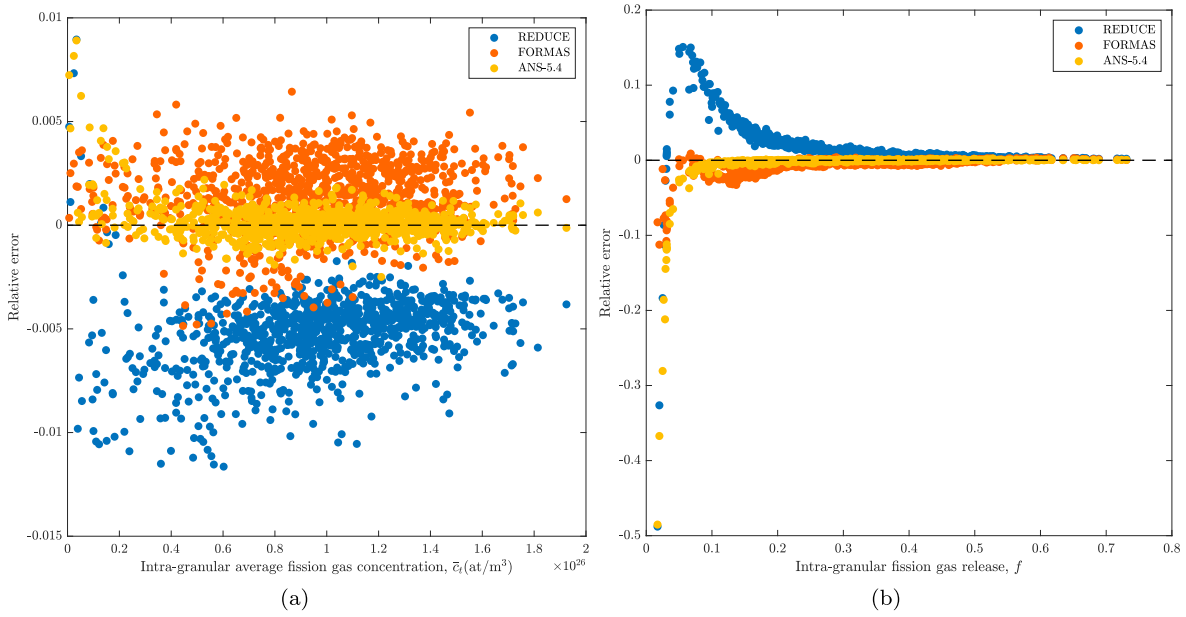

Fig. 15. Comparison between REDUCE, FORMAS, and ANS-5.4 algorithms in terms of relative error with respect to the reference algorithm. Each point corresponds to a calculation with randomly generated conditions.

characteristics mentioned above, i.e., the high number of modes. The current version of REDUCE does not apply any dedicated correction for this regime, since being developed targeting application in fast reactor conditions, the range of low fission gas release is not a priority at this stage of the development.

In Fig. 14, it is possible to appreciate the computational times taken by the three algorithms. As expected, the REDUCE algorithm takes longer to complete the simulation than the FORMAS algorithm, about 1.2 times longer, since the version of FORMAS used in this work with four exponential terms solves four decoupled ODEs that are computationally more efficient than solving a system of five coupled ODEs. On the other side results that the REDUCE algorithm has a computational cost about 1.6 times lower than the ANS-5.4 algorithm having to solve in this case thirty spatial modes that correspond to thirty decoupled ODEs. The computational time of REDUCE appears thus to be in line with the requirements of fuel performance codes.

To investigate in finer detail the accuracy of the three algorithms in Fig. 15 we show the relative error of the solution obtained with each algorithm with respect to a reference solution. This reference solution is obtained by increasing the number of modes of the ANS-5.4 algorithm so that it is sufficiently high to ensure that the truncation error is negligible, moreover each time interval has been discretized in 5000 sub-steps compared to the 1000 sub-steps used for the solution through the proposed algorithms [53]. Focusing on Fig. 15a, it is possible to see that the accuracy of REDUCE algorithm is comparable than that of FORMAS and ANS-5.4, showing a relative error below one percent in more than 90% of the analyzed random histories. The maximum discrepancy occurs in correspondence of the histories characterized by strong variations of temperature and fission rate values due to the different implementation characteristics of the three algorithms. As mentioned, the FORMAS

algorithm was implemented in time-varying conditions therefore manages to better capture the sharp change of parameters instead the quasi-exact ANS-5.4 algorithm, although it has been implemented in constant conditions, good accuracies are obtained in time-varying situations thanks to the high number of modes used. We can therefore conclude that, although the reduced order model has been derived and implemented for application in constant conditions, it is capable of a complete description of the diffusive phenomenon in a wide range of situations, as the FORMAS and ANS-5.4 algorithms do. In Fig. 15b is possible to see more in detail the discrepancy already depicted in Fig. 13 which occurs most in correspondence of the histories characterized by low fission gas values, which as mentioned are those of least interest for application in fast reactor conditions. Remarkably, the relative error associated with the REDUCE algorithm is highly consistent over the whole range of intra-granular fission gas release, despite not being subject to any correction for $f < 0.1$.

7. Conclusions and future developments

In this paper, a novel approach based on reduced order modelling is developed to solve the problem of intra-granular fission gas diffusion inside spherical and cylindrical grains, in terms of average intra-granular gas concentration. The aim of this work is to construct a numerical model that is applicable in fuel performance codes and that allows overcoming the hypotheses of spherical grains and uniform temperature and fission rate assumed in state-of-the-art algorithms. The proposed reduced order model employs the proper orthogonal decomposition technique to select the most energetic modes of the intra-granular gas concentration from *snapshots* of an high-fidelity solution of the problem. The solution of the gas diffusion problem (i.e., the average intra-granular gas concentration evolution in time) is reconstructed as combination of these modes, for both spherical and cylindrical grain geometry.

When compared to state-of-the-art algorithms for the diffusion of fission gas in spherical grains (FORMAS and ANS-5.4), the proposed reduced order model shows satisfactory performances, both in terms of accuracy and of computational time. Thus, this methodology is in line with the current requirements of fuel performance codes.

Where the proposed reduced order modelling methodology shines is in the application to the problem of diffusion in columnar grains, which can not be approached with state-of-the-art algorithms. The model can also be adapted to solve more general formulations of fission gas behaviour, for instance, including terms for bubble motion and/or nucleation. The integration of the proposed reduced order model in fuel performance codes is the natural extension of the present work. This further development is potentially challenging since the typical size of columnar grains is larger than the standard mesh cells used in fuel performance simulations, which may require a dedicated coupling scheme between the fission gas behaviour model and the fuel performance code itself.

After its integration in fuel performance codes, the integral validation of the proposed model to demonstrate its capabilities in providing consistent results will be carried out through the assessment of several fuel rod irradiation experiments. In particular, the spherical reduced order model will be validated through the GE7 irradiation experiment from the Risø-3 experimental program, included in the IAEA FUMEX-III Project [56–58] instead the available validation database on the SUPERFACT-1 irradiation experiment [59,60] will be considered for the cylindrical model.

Summarizing, the main outcome of this work is the application of the reduced order methodology to the fission gas diffusion problem in columnar (cylindrical) grains, improving the physics-based description of nuclear fuel behaviour in fast reactors within engineering tools. The proposed methodology of developing reduced order models to be introduced within fuel performance codes can be extended to other fuel concepts (e.g., uranium silicide fuel grains) and to other phenomena besides fission gas behaviour (e.g., hydrogen precipitation in the cladding). The current version of the proposed reduce order models have been implemented in the SCIANTIX code.

Declaration of competing interest

The authors declare that they have no known competing financial interests or personal relationships that could have appeared to influence the work reported in this paper.

Acknowledgments

This research activity has received funding from the Euratom research and training programme 2017-2021 through the INSPYRE Project under grant agreement No.754329 and from the Euratom research and training programme 2020-2024 through the PATRICIA project under grant agreement No.945077. The authors are grateful to A.G. Carloni.

References

[1] D.R. Olander, Fundamental Aspects of Nuclear Reactor Fuel Elements, Technical Information Center – Energy Research and Development Administration, University of California, Berkeley, CA, USA, 1976.
[2] H.J. Matzke, Gas release mechanisms in UO_2 – a critical review, Radiat. Eff. 53 (1980) 219–242, https://doi.org/10.1080/00337578008207118.
[3] R.J. White, M.O. Tucker, A new fission-gas release model, J. Nucl. Mater. 118 (1) (1983) 1–38, https://doi.org/10.1016/0022-3115(83)90176-9.
[4] R.J. White, The development of grain-face porosity in irradiated oxide fuel, J. Nucl. Mater. 325 (2004) 61–77, https://doi.org/10.1016/j.jnucmat.2003.10.008.
[5] P. Van Uffelen, R.J.M. Konings, C. Vitanza, J. Tulenko, Analysis of reactor fuel rod behavior, in: D.G. Cacuci (Ed.), Handbook of Nuclear Engineering, vol. 13, Springer Science + Business Media, LLC., New York, NY, USA, 2010, pp. 1519–1627, https://doi.org/10.1007/978-0-387-98149-9-13.
[6] G. Pastore, L. Luzzi, V. Di Marcello, P. Van Uffelen, Physics-based modelling of fission gas swelling and release in UO_2 applied to integral fuel rod analysis, Nucl. Eng. Des. 256 (2013) 75–86, https://doi.org/10.1016/j.nucengdes.2012.12.002.
[7] T.M. Besmann, et al., State-of-the-art report on multi-scale modelling of nuclear fuels. www.oecd-nea.org, 2015.
[8] P.V. Uffelen, J. Hales, W. Li, G. Rossiter, R. Williamson, A Review of Fuel Performance Modelling, vol. 4, 2019, https://doi.org/10.1016/j.jnucmat.2018.12.037.
[9] K. Lassmann, Transuranus: a fuel rod analysis code ready for use, J. Nucl. Mater. 188 (1992) 295–302, https://doi.org/10.1016/0022-3115(92)90487-6.
[10] M. Lainet, B. Michel, J.C. Dumas, M. Pelletier, I. Ramière, Germinal, a fuel performance code of the pleiades platform to simulate the in-pile behaviour of mixed oxide fuel pins for sodium-cooled fast reactors, J. Nucl. Mater. 516 (2019), https://doi.org/10.1016/j.jnucmat.2018.12.030.
[11] G. Thouvenin, B. Michel, J. Sercombe, D. Plancq, P. Thevenin, Multidimensional Modeling of a Ramp Test with the Pwr Fuel Performance Code Alcyone, 2007.
[12] D.M. Perez, R.L. Williamson, S.R. Novascone, T.K. Larson, J.D. Hales, B. W. Spencer, G. Pastore, An Evaluation of the Nuclear Fuel Performance Code bison, vol. 2, 2013.
[13] K. Forsberg, A.R. Massih, Fission gas release under time-varying conditions, J. Nucl. Mater. 127 (1985) 141–145, https://doi.org/10.1016/0022-3115(85)90348-4.
[14] P. Hermansonn, A.R. Massih, An effective method for calculation of diffusive flow in spherical grains, J. Nucl. Mater. 304 (2002) 204–211, https://doi.org/10.1016/S0022-3115(02)00873-5.
[15] K. Lassmann, H. Benk, Numerical algorithms for intragranular fission gas release, J. Nucl. Mater. 280 (2000) 127–135, https://doi.org/10.1016/S0022-3115(00)00044-1.
[16] C. Rim, Background and Derivation of ANS-5.4 Standard Fission Product Release Model, Tech. Rep. NUREG/CR-2507, 1982.
[17] W.N. Rausch, F.E. Panisko, ANS-5.4: a Computer Subroutine for Predicting Fission Gas Release, Tech. Rep. NUREG/CR-0497, Pacific Northwest Laboratory, USA, 1979, p. 8.
[18] J. Turnbull, C. Beyer, Background and Derivation of ANS-5.4 Standard Fission Product Release Model, United States Nuclear Regulatory Commision, 2010, https://doi.org/10.2172/1033086.
[19] P. Elton, K. Lassmann, Calculational methods for diffusional gas release, Nucl. Eng. Des. 101 (3) (1987) 259–265, https://doi.org/10.1016/0029-5493(87)90054-9.
[20] D. Pizzocri, C. Rabiti, L. Luzzi, T. Barani, P. Van Uffelen, G. Pastore, Polypole-1: an accurate numerical algorithm for intra-granular fission gas release, J. Nucl. Mater. 478 (2016) 333–342, https://doi.org/10.1016/j.jnucmat.2016.06.028.
[21] G. Pastore, D. Pizzocri, C. Rabiti, T. Barani, P. Van Uffelen, L. Luzzi, An effective numerical algorithm for intra-granular fission gas release during non–equilibrium trapping and re-solution, J. Nucl. Mater. 509 (2018) 687–699, https://doi.org/10.1016/j.jnucmat.2018.07.030.

[22] D. Pizzocri, G. Pastore, T. Barani, A. Magni, L. Luzzi, P. Van Uffelen, S. Pitts, A. Alfonsi, J. Hales, A model describing intra-granular fission gas behaviour in oxide fuel for advanced engineering tools, J. Nucl. Mater. 502 (2018) 323–330.
[23] N.E. Todreas, M. Kazimi, Nuclear Systems, vol. I, CRC Press, 2012, https://doi.org/10.1201/b14887.
[24] A.E. Waltar, D.R. Todd, P.V. Tsvetkov, Fast spectrum reactors 9781441995728 (2012), https://doi.org/10.1007/978-1-4419-9572-8.
[25] S.J. Zinkle, K.A. Terrani, J.C. Gehin, L.J. Ott, L.L. Snead, Accident tolerant fuels for LWRs: a perspective, J. Nucl. Mater. 448 (1–3) (2014) 374–379, https://doi.org/10.1016/j.jnucmat.2013.12.005.
[26] T. Barani, G. Pastore, D. Pizzocri, D. Andersson, C. Matthews, A. Alfonsi, K. Gamble, P. Van Uffelen, L. Luzzi, J. Hales, M ultiscale modeling of fission gas behavior in u3si2 under lwr conditions, J. Nucl. Mater. 522 (2019) 97–110, https://doi.org/10.1016/j.jnucmat.2019.04.037. https://www.sciencedirect.com/science/article/pii/S0022 311519301151. URL.
[27] T. Lassila, A. Manzoni, A. Quarteroni, G. Rozza, Model Order Reduction in Fluid Dynamics: Challenges and Perspectives, Reduced Order Methods for Modeling and Computational Reduction, Springer International Publishing, 2014, pp. 235–273, https://doi.org/10.1007/978-3-319-02090-7-9.
[28] A. Manzoni, A. Quarteroni, G. Rozza, Computational reduction for parametrized PDEs: strategies and applications, Milan J. Math. 80 (2012) 283–309, https://doi.org/10.1007/s00032-012-0182-y.
[29] J. Lumley, The structure of inhomogeneous turbulent flows, in: Proceedings of the International Colloquium, vol. 80, Publishing house Nakua, 1967, pp. 166–167.
[30] L. Sirovich, Turbulence and the dynamics of coherent structures part I-III, Q. Appl. Math. 45 (1987) 561–571.
[31] P. Holmes, J. Lumley, G. Berkooz, Turbulence, Coherent Structures, Dynamical Systems and Symmetry, Cambridge University Press, 1996, https://doi.org/10.1017/cbo9780511622700.
[32] D. Pizzocri, T. Barani, L. Luzzi, SCIANTIX: a new open source multi-scale code for fission gas behaviour modelling designed for nuclear fuel performance codes, J. Nucl. Mater. 532 (2020), https://doi.org/10.1016/j.jnucmat.2020.152042.
[33] D. Pizzocri, T. Barani, L. Luzzi, SCIANTIX code. https://gitlab.com/poliminrg/sciantix, 2020.
[34] V. Di Marcello, V. Rondinella, A. Schubert, J. Van De Laar, P. Van Uffelen, Modelling actinide redistribution in mixed oxide fuel for sodium fast reactors, Prog. Nucl. Energy 72 (2014), https://doi.org/10.1016/j.pnucene.2013.10.008.
[35] S. Novascone, P. Medvedev, J.W. Peterson, Y. Zhang, J. Hales, Modeling porosity migration in LWR and fast reactor mox fuel using the finite element method, J. Nucl. Mater. 508 (2018), https://doi.org/10.1016/j.jnucmat.2018.05.041.
[36] T. Barani, D. Pizzocri, F. Cappia, G. Pastore, L. Luzzi, P. Van Uffelen, M odeling high burnup structure in oxide fuels for application to fuel performance codes. part ii: porosity evolution, J. Nucl. Mater. 563 (2022), 153627, https://doi.org/10.1016/j.jnucmat.2022.153627. https://www.sciencedirect.com/science/article/pii/S0022 311522001234. URL.
[37] D.R. Olander, Theory of helium dissolution in uranium dioxide. II. Helium solubility, J. Chem. Phys. 43 (3) (1965) 785–788, https://doi.org/10.1063/1.1696844.
[38] A. Booth, A Method of Calculating Fission Gas Diffusion from UO_2 Fuel and its Application to the X-2-F Loop Test, Atomic energy of Canada Limited, 1957.
[39] M. Speight, A calculation on the migration of fission gas in material exhibiting precipitation and re-solution of gas atoms under irradiation, Nucl. Sci. Eng. 37 (1969) 180–185, https://doi.org/10.13182/nse69-a20676, 180–185. 37.
[40] J. Noirot, L. Desgranges, J. Lamontagne, Detailed characterisations of high burn-up structures in oxide fuels, J. Nucl. Mater. 372 (2008), https://doi.org/10.1016/j.jnucmat.2007.04.037.
[41] L. Noirot, M argaret: a comprehensive code for the description of fission gas behavior, Nuclear Engineering and Design, in: (W3MDM) University of Leeds International Symposium: what where when? Multi-Dimensional Advances for Industrial Process Monitoring, vol. 241, 2011, pp. 2099–2118, https://doi.org/10.1016/j.nucengdes.2011.03.044, 6, https://www.sciencedirect.com/science/article/pii/S0029 549311002561. URL.
[42] A. Cheniour, G. Pastore, J.M. Harp, C.M. Petrie, N.A. Capps, A pplication of bison to uo2 minifuel fission gas release analysis, J. Nucl. Mater. 565 (2022), 153686, https://doi.org/10.1016/j.jnucmat.2022.153686. https://www.sciencedirect.com/science/article/pii/S0022.311522001799. URL.
[43] V. Tarasov, M. Veshchunov, M odels for fuel porosity evolution in uo2 under various regimes of reactor operation, Nucl. Eng. Des. 272 (2014) 65–83, https://doi.org/10.1016/j.nucengdes.2014.02.016. https://www.sciencedirect.com/science/article/pii/S0029.549314001095. URL.
[44] OpenFOAM®-foundation, Openfoam version 8.0. https://openfoam.org, 2017.
[45] J.A. Turnbull, C.A. Friskney, J.R. Findlay, F.A. Johnson, A.J. Walter, The diffusion coefficients of gaseous and volatile species during the irradiation of uranium dioxide, J. Nucl. Mater. 107 (1982) 168–184, https://doi.org/10.1016/0022-3115(82)90419-6.
[46] J.A. Turnbull, R. White, C. Wise, The Diffusion Coefficient for Fission Gas Atoms in Uranium Dioxide, International Atomic Energy Agency, 1989, pp. 174–181.
[47] S. Lorenzi, A. Cammi, L. Luzzi, G. Rozza, POD-Galerkin method for finite volume approximation of Navier–Stokes and RANS equations, Comput. Methods Appl. Mech. Eng. 311 (2016) 151–179, https://doi.org/10.1016/j.cma.2016.08.006.
[48] G. Berkooz, P. Holmes, J. Lumley, The proper orthogonal decomposition in the analysis of turbulent flows, Annu. Rev. Fluid Mech. 25 (1993) 539–575, https://doi.org/10.1146/annurev.fl.25.010193.002543.
[49] S. Sirisup, G.E. Karniadakis, Stability and accuracy of periodic flow solutions obtained by a pod-penalty method, Phys. Nonlinear Phenom. 202 (3–4) (2005) 218–237, https://doi.org/10.1016/j.physd.2005.02.006.
[50] G. Pastore, L.P. Swiler, J.D. Hales, S.R. Novascone, D.M. Perez, B.W. Spencer, L. Luzzi, P. Van Uffelen, R.L. Williamson, Uncertainty and sensitivity analysis of fission gas behavior in engineering-scale fuel modeling, J. Nucl. Mater. 465 (2015) 398–408, https://doi.org/10.1016/j.jnucmat.2014.09.077.
[51] R.L. Williamson, J.D. Hales, S.R. Novascone, M.R. Tonks, D.R. Gaston, C. J. Permann, D. Andrs, R.C. Martineau, Multidimensional multiphysics simulation of nuclear fuel behavior, J. Nucl. Mater. 423 (2012) 149–163.
[52] P. Lösönen, On the behaviour of intragranular fission gas in UO_2 fuel, J. Nucl. Mater. 280 (2000) 56–72.
[53] G. Zullo, D. Pizzocri, L. Luzzi, On the Use of Spectral Algorithms for the Prediction of Short-Lived Volatile Fission Product Release: Methodology for Bounding Numerical Error, Nuclear Engineering and Technology, 2021.
[54] J.A. Turnbull, R. Cornell, The re-solution of fission-gas atoms from bubbles during the irradiation of UO_2 at an elevated temperature, J. Nucl. Mater. 41 (1971) 156–160, https://doi.org/10.1016/0022-3115(71)90075-4.
[55] F.S. Ham, Theory of diffusion-limited precipitation, J. Phys. Chem. Solid. 6 (1958) 335–351, https://doi.org/10.1016/0022-3697(58)90053-2.
[56] S. Boneva, R. Calabrese, G. Chassie, D. Chulkin, A. Denis, The Third RISø Fission Gas Project: Bump Test GE7 (ZX115), Tech. Rep. RISØ-FGP3-GE7, 1990.
[57] Fuel Modelling at Extended Burnup (FUMEX-II), Tech. Rep. IAEA-TECDOC-1687, 2012.
[58] Improvement of Computer Codes Used for Fuel Behaviour Simulations (FUMEX-III), Tech. Rep. IAEA-TECDOC-1697, 2013.
[59] L. Luzzi, T. Barani, B. Boer, L. Cognini, A.D. Nevo, M. Lainet, S. Lemehov, A. Magni, V. Marelle, B. Michel, D. Pizzocri, A. Schubert, P.V. Uffelen, M. Bertolus, Assessment of three european fuel performance codes against the superfact-1 fast reactor irradiation experiment, Nucl. Eng. Technol. 53 (2021), https://doi.org/10.1016/j.net.2021.04.010.
[60] L. Luzzi, T. Barani, B. Boer, A.D. Nevo, M. Lainet, S. Lemehov, A. Magni, V. Marelle, B. Michel, D. Pizzocri, A. Schubert, P.V. Uffelen, M. Bertolus, Assessment of inspyre-extended fuel performance codes against the superfact-1 fast reactor irradiation experiment, Nucl. Eng. Technol. (2022), https://doi.org/10.1016/j.net.2022.10.038.